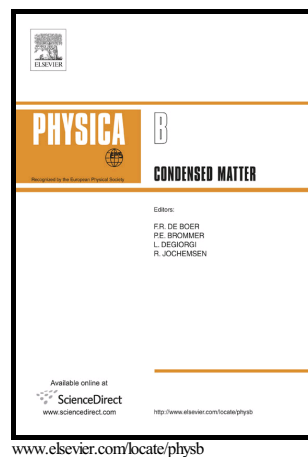


Author's Accepted Manuscript

Studies on synthesis, structural, luminescent and thermal properties of a new non-linear optical crystal: 4-amino-4H-1,2,4-triazol-1-ium-3-hydroxy-2,4,6-trinitrophenolate

P. Dhamodharan, K. Sathya, M. Dhandapani



PII: S0921-4526(16)30577-4
DOI: <http://dx.doi.org/10.1016/j.physb.2016.12.009>
Reference: PHYSB309750

To appear in: *Physica B: Physics of Condensed Matter*

Received date: 30 September 2016

Accepted date: 6 December 2016

Cite this article as: P. Dhamodharan, K. Sathya and M. Dhandapani, Studies on synthesis, structural, luminescent and thermal properties of a new non-linear optical crystal: 4-amino-4H-1,2,4-triazol-1-ium-3-hydroxy-2,4,6-trinitrophenolate, *Physica B: Physics of Condensed Matter* <http://dx.doi.org/10.1016/j.physb.2016.12.009>

This is a PDF file of an unedited manuscript that has been accepted for publication. As a service to our customers we are providing this early version of the manuscript. The manuscript will undergo copyediting, typesetting, and a review of the resulting galley proof before it is published in its final citable form. Please note that during the production process errors may be discovered which could affect the content, and all legal disclaimers that apply to the journal pertain.

Studies on synthesis, structural, luminescent and thermal properties of a new non-linear optical crystal: 4-amino-4*H*-1,2,4-triazol-1-ium-3-hydroxy-2,4,6-trinitrophenolate

P. Dhamodharan, K. Sathya and M. Dhandapani*

Department of Chemistry, Sri Ramakrishna Mission Vidyalaya College of Arts and Science, Coimbatore-641 020, Tamil Nadu, India.

*Corresponding author's ; Phone: +91 94420 01232. srmvdhandapani@gmail.com

Abstract:

A new organic proton transfer complex having NLO activity, 4-amino-4*H*-1,2,4-triazol-1-ium-3-hydroxy-2,4,6-trinitrophenolate (ATHTP), was crystallized to investigate the factors which stabilize the structure of the crystal. The compound crystallizes in triclinic system with space group P-1. Elemental analysis, Thermal analysis, UV-Vis-NIR, FT-IR and NMR spectral analyses were carried out to characterize the crystal. Optical, spectral and thermal properties of the title crystal were analyzed to recommend the material for optical useful applications. Z-scan was used to measure the effective third-order nonlinear optical susceptibility and nonlinear refractive index. The crystal structure was exploited using single crystal XRD and the obtained structure was optimized using Gaussian 09 program B3LYP/6-311++G(d,p) level of basis set. This hydrogen bond interactions leads to the increase in hyperpolarizability of ATHTP and was 30 times greater than that of urea. Hirshfeld analyses were carried out to explore covalent and non covalent interactions.

Keywords:

Single crystal XRD, Phosphorescence, Hydrogen bonding, Hirshfeld, Hyperpolarizability.

1. Introduction

Supramolecular architectures assembled from numerous delicate non-covalent interactions like hydrogen bonds, π - π^* stacking and electrostatic interactions etc., have large interest in their wide applications in life and materials science [1, 2]. Intermolecular interactions are really exciting to explore in any molecular material. An in-depth analysis of these interactions becomes handy when the material is in the crystalline form. Organic materials are attractive due to their electronic and optical properties and the molecular structure can be easily modified for suitable applications. The growth of single crystals has gained much important for the fabrication of technologically important devices. Triazoles and nitro phenols are capable of forming predictable hydrogen bonding arrangements. Nitrophenols and their derivatives like dinitrophenols and trinitrophenols can transfer proton to some inorganic and organic bases to form stable molecular adducts. In these complexes, phenoxide ion enhances electron donating character to positively charged partner increasing hyperpolarizability. Number organic crystals formed between picric acid and triazole derivatives have been thoroughly studied in the recent past due to their large second order optical nonlinearities, inherent ultra fast response time and large optical threshold satisfying the technology requirements. Styphnic acid, otherwise known as 2,4,6-trinitrobenzene-1,3-diol, is an interesting analogue of picric acid [3-6]. Investigations on molecular adducts synthesized from triazoles and styphnic acid are scarce in literature.

In this research work, we report for the first time structural, spectral characterizations and optical investigations of a new organic NLO material, 4-amino-4*H*-1,2,4-triazol-1-ium-3-hydroxy-2,4,6-trinitrophenolate.

2. Experimental section

2.1. Synthesis

Styphnic acid was prepared by nitrating the resorcinol following Tadeusz Urbanski's et al's procedure [7]. The reaction scheme is outlined step-1 of Figure 1. The chemicals used in the synthesis were of analar grade (Sigma-Aldrich). The final product was recrystallized several times to achieve superior quality. 4-amino-4*H*-1,2,4 triazole and laboratory synthesized 2,4,6-trinitrobenzene-1,3-diol (styphnic acid) were dissolved in methanol in 1:1 stoichiometric proportions separately and the two solutions were mixed to get a yellow color precipitate. Yellow colored ATHTP crystals were obtained by solution growth-solvent evaporation technique after ten days. The reaction scheme is shown in the step-2 of Figure 1. Elemental analysis confirmed the elemental proportions C, H, N analysis: C₈H₇N₇O₈ (M.W: 329.21), Calculated result (%): C, 29.19; H, 2.14; N, 29.78; Found: C, 29.12; H, 2.21; N, 29.56. Important functional groups and formation of the compound were confirmed by FT-IR spectroscopic techniques. IR (KBr) (cm⁻¹) selected bonds: $\nu=3365$ (s) (Ar-OH), 3140 (s) (Ar-NH), 2983 (s) (-CH), 1578 (m) (NO₂)_{asy}, 1341 (m) (NO₂)_{sy}, 1286 (m) (C-N), 1296 (m) (C-O).

2.2. Characterization techniques

Elemental analysis (CHN) was performed in a flash EA 1112 full automatic trace element analyzer. The Fourier-transform infrared spectrum of ATHTP was recorded in the region 4000-400 cm⁻¹ by JASCO FT/IR 5300 infrared spectrophotometer. The optical transmittance of solid material was measured in a JASCO (V-570) UV/VIS/NIR spectrophotometer. Photoluminescence spectrum of ATHTP crystal was recorded in the wavelength range of 440-700 nm using Horiba Jobin-Yvon-FL3-22 Fluorolog spectrofluorometer.

^1H , ^{13}C and DEPT-135 NMR spectra were recorded in a Bruker Avance 400 MHz FT-NMR spectrophotometer with tetramethylsilane as an internal standard using $\text{DMSO-}d_6$ as the solvent. Thermal analyses (TG/DTA) were performed by a Mettler Toledo Star SW 8.10 TG/DTA thermal analyzer in the range 30-800°C under nitrogen atmosphere at a heating rate of 20°C per minute. Single crystal data were collected using Oxford XCalibur, Gemini diffractometer equipped with EOS CCD detector at 25°C using $\text{MoK}\alpha$ radiations (0.71073 Å). The data were reduced using CrysAlis^{Pro} Software and absorption correction using multi Ψ -scans. Structure was solved using SHELXS-97 and refined by full-matrix least squares against F^2 using SHELXL-97 software [8, 9]. Non-hydrogen atoms were refined with anisotropic thermal parameters. Third-order NLO property of ATHTP was investigated using z-scan technique and in this measurement, a He-Ne laser ($\lambda = 632.8$ nm) was used as the light source.

3. Computational Details

The molecular structure of ATHTP in the ground state was optimized and the structural parameters have been computed using Gaussian 09 program package at the Becke3-Lee-Yang-Parr (B3LYP) level with 6-311++G(d,p) basis set [10-13]. First-order hyperpolarizability calculations have been performed using Gaussian 09 program.

4. Results and Discussion

4.1. Structural Analysis

Single crystal data were collected using Oxford XCalibur, Gemini diffractometer equipped with EOS CCD detector at 25°C using $\text{MoK}\alpha$ radiations (0.71073 Å). The compound, ATHTP, crystallizes in triclinic system. The lattice parameters are $a = 7.8000(16)$ Å, $b = 8.9000(18)$ Å, $c = 9.932(2)$ Å, $\alpha = 87.22(3)^\circ$, $\beta = 75.97(3)^\circ$ and $\gamma = 66.30(3)^\circ$. The unit cell

volume (V) is = $611.5(2) \text{ \AA}^3$ and the number of molecules in unit cell (Z) is 2. The asymmetric unit consists 4-amino-4*H*-1,2,4-triazolium moiety and styphnate moiety conforming a proton migration from styphnic acid to 4-amino-4*H*-1,2,4-triazol during synthesis.

The C(3)-(O8) bond length (1.328 \AA) is a little shorter than found in phenols, (1.36 \AA), which is due to delocalization of the pair of electrons of oxygen onto the adjacent nitro groups in the styphnate moiety [14]. The C-C-C bond angles at Carbon atoms having nitro groups as substituents are notably larger than those at C atoms having H atoms as substituents. Bent et al [15] explained by the strong electron attracting power of the nitro group reducing the s character of the C σ orbital to the N atom and increasing s character of the C σ orbital to the adjacent C atoms, thus causing the bond angles to be greater than 120° . In agreement with these observations, the nitro group substituted C atoms in ATHTP have C-C-C bond angles of 127.20° at C (2) and 122.4° at C (6). The lone hydrogen substituted ring C atom has a C-C-C bond angle of 121.1° . The pair of electrons on O (8) of the ring is conjugated with a π bond on the benzene ring, causing the C(3)-(O8) bond length to be shortened and the C-C(3)-C bond angle to be less than 120° .

The crystal structure is stabilized by the presence of various covalent bonds and hydrogen bonds like C-H...O, N-H...O and also bifurcated hydrogen bonds. Hydrogen (H1) atom of styphnate moiety forms bifurcated hydrogen bonding with neighbouring oxygen atom (O1) of nitro group in the other styphnate moiety and ring nitrogen atom (N5) of triazole moiety through C-H...O and C-H...N hydrogen bonding. Another hydrogen bond occurs between oxygen atom (O5) of the styphnate and -CH (C7-H2) of the triazole moiety through C7-H2...O5 hydrogen bonding. The amino N(7)-H(5b) also participates in the N-H...O hydrogen bonding with oxygen atom (O3) of nitro group in styphnate moiety. In the ATHTP crystal structure, one of the nitro

groups (O1-N1-O2) is largely deviated from the plane of the benzene ring with an angle of 71.97°. The ORTEP, crystal packing diagram, crystallographic data and structural geometrical parameters of ATHTP are given in Figures. 2, 3 and Tables 1, 2, respectively.

4.2. UV-Vis-NIR spectral analysis

The recorded UV-Vis absorption spectrum of ATHTP in methanol solvent is shown in Figure S1. The spectrum exhibits charge transfer π - π^* and n - π^* bands of styphnic acid and 4-amino-4*H*-1,2,4-triazole moieties of the proton transfer complex salt. This charge transfer arises due to the promotion of fractional negative charge from donor to the acceptor molecule (i.e. styphnic acid molecule to the 4-amino-4*H*-1,2,4-triazole molecule) and appears on the longer wavelength side of the spectrum at 392 nm. This band confirms the presence of intermolecular charge transfer activity in ATHTP. The n - π^* band of 4-amino-4*H*-1,2,4-triazole in the complex salt appears at 258 nm. The π - π^* transition of styphnic acid appears at 358 nm.

UV-Vis-NIR transmittance spectrum of ATHTP recorded in the solid state is shown in Figure 4. The transmittance of grown crystal ATHTP was recorded in the range 200-1400 nm. There is no considerable absorption of light within the entire visible range. The lower cut off of the grown crystal is around 290 nm and it is an essential parameter for frequency doubling process using diode and solid state laser [16]. The absence of the absorption in the visible range of the crystal is incredibly helpful in opto electronic applications.

4.3. Photoluminescent properties

Fluorescence occurs generally in molecules that are aromatic or having conjugated double bonds with a high degree of resonance stability. The study of photoluminescence is of great current interest because of its applications in chemical sensors, photo chemistry and

electroluminescent display. The powdered sample of ATHTP was significantly more intense green emission in the electro-magnetic spectrum with a maximum at 490 nm ($\lambda_{\text{ex}} = 440$ nm). It shows an efficient luminescence in the longer wavelength ranges it shown in Figure 5. The results indicate that the ATHTP crystal has a green emission property suggesting that it can be used for display and solid-state lightening applications [17].

4.4. Thermal analysis

The TG/DTA thermogram (Figure 6) of ATHTP exhibits no thermal events till 178°C before the start of the decomposition illustrating the absence of physically adsorbed or lattice water in the crystal. The DTA curve of ATHTP shows an endothermic peak at 178 °C which can be attributed to the melting point of the sample. The sharpness of endothermic peak shows the good degree of crystallinity and purity of the sample. The TG curve shows that a single stage weight loss (>85%) occurring between 178 °C and 500°C. With temperature increasing, volatile substances such as ammonia and CH₄, NO₂ and CO molecule get liberated. The final residue is carbon.

4.5. NMR Spectral Studies

¹H and ¹³C NMR spectra were recorded with tetramethylsilane as an internal standard using DMSO-*d*₆ as the solvent which are shown in Figure 7. The ¹H NMR spectrum of the ATHTP shows three proton signals indicating the presence of three different proton environments in the molecule. The δ value of C(5)-H proton is observed in up field at δ 8.6 ppm in styphnate moiety. The singlet at δ 6.8 ppm is due to the presence of -NH₂ proton of triazole moiety. The peak at δ 9.5 ppm is due to presence of two -CH protons present in triazole moiety. The solvent peak is observed at δ 2.5 ppm for DMSO-*d*₆ solvent. The N-H⁺ proton of triazole

moiety in the complex is far downfield shifted and does not appear in the spectrum [18]. The signal for hydroxyl proton is also far shifted to downfield which is also not seen in the spectrum due to deshielding effect of oxygen atom [19].

In general, aromatic carbons give signals with chemical shift values from 100 to 200 ppm [20]. The experimental chemical shifts of the compound occur in the range of δ 125.8-156.1 ppm. The external magnetic field experienced by the carbon nuclei is affected by the electronegativity of the atoms attached to them. The chemical shift of equivalent carbons (C1, C3) is observed in the downfield at δ 156.1 ppm due to their attachment with more electronegative oxygen atom. The carbon atoms C4 and C6 are chemically equivalent so the lone signal for these two carbon atoms occurs at δ 135.4 ppm. The signal for C2 carbon which is attached to nitro group appears at δ 125.8 ppm. The chemical shift of C5 carbon atom appears at 126.2 ppm. The other signal observed at δ 144.4 ppm is due to presence of two chemically equivalent carbons (C7, C8) present in the triazole moiety. The solvent peak (DMSO-d₆) is observed at around δ 40 ppm.

Presence of different types of -CH, CH₂ and CH₃ carbons can be clearly identified using DEPT-135 spectral analysis. The signals observed at δ 126.2 and 144.4 ppm are due to CH (C5) of styphnate moiety and CH (C7, C8) of triazole moiety. The DEPT-135 NMR spectrum of ATHTP is shown in Figure S2.

4.6. Optimized geometry

The optimized molecular structure of ATHTP was calculated using, B3LYP/6-311++G(d,p) level of basis set. It is found that most of the optimized bond lengths are slightly higher than the experimental values. The deviations can be attributed to the fact that the theoretical calculations were performed assuming isolated molecules in the gaseous phase and the experiments were conducted using crystals [21, 22].

The molecule is stabilized by inter- and intra-molecular hydrogen bonding. Out of the three hydrogen bond interactions, N-H...O and C-H...O are found to be intermolecular in nature. The O-H...O hydrogen bond is intramolecular. The molecular structure of ATHTP with atom numbering scheme adopted in the computations is given in Figure 8.

The dihedral angle of 159.6° pertaining to C13-C19-N10-O24 and -18.6° to C13-C19-N10-O23 confirm that the nitro group is coplanar with phenyl ring. The hydrogen bond distance of O25-H26...O23 (2.48\AA) and O-H-O angle (146.5°) confirm O-H...O intramolecular hydrogen bonding. The decrease in endocyclic angle C19-C9-C16 (113.9°) and increase in exocyclic angles C16-C9-O27 (123.5°) and C19-C9-O27 (122.4°) from expected 120° confirms the intermolecular hydrogen bonding in the ring moiety.

O27 of the styphnate forms bifurcated hydrogen bonds O27...H29-N4 and O27...H28-C6 with the triazole moiety. (H28) of triazole moiety also participates in the bifurcated hydrogen bond with two oxygen atoms (O24 and O27) of styphnate moiety viz., C6-H28...O24 and C6-H28...O27. The elongation of N4-H29 and N1-C7 bond length values compared to other N-C and N-H bonds confirms the formation of intermolecular hydrogen bonding, O27...H29-N4. There is an increase in bond length of N4-H29, viz., 1.37\AA due to hydrogen bonding whereas the bond length of N4-H30 is unaffected (1.032\AA).

4.7. Hyperpolarizability calculations

Quantum chemical methods were used for assessing the molecular NLO property of ATHTP. Hyperpolarizability is useful in understanding the relationship of the structure depended their nonlinear properties. Polarizability (α_0) and first-order hyperpolarizability (β) of ATHTP were calculated using B3LYP/6-311++G(d,p) level of basis set. The calculated β value is very useful as this clearly indicates the direction of charge delocalization or polarization. The

calculated first-order polarizability (β) and the ground state dipole moment (μ_g) of synthesized crystal is 3.89×10^{-30} esu. Table 4 shows that β_{tot} has the largest calculated value for ATHTP crystal while β_{tot} is comparably decreased for the constituents such as styphnic acid and 4-amino-4H-1,2,4-triazole of the ATHTP crystal. The total first-order polarizability (β) in the ATHTP crystal is approximately 30 times greater than that of urea (0.13×10^{-30} esu). Comparison of static first hyperpolarizability for the constituents of ATHTP is shown in Table 3.

4.8. Hirshfeld surface analysis

Hirshfeld surface depends on the geometry of the molecules, orientation of the molecules in the neighborhood and the nature of atoms that make close contacts in the chosen molecule. In other words, it gives a detailed explanation on the immediate environment of a molecule in a crystal. For each point on the surface, two distances are defined; d_e , the distance from the point to the nearest nucleus external to the surface and d_i , the distance to the nearest nucleus internal to the surface. These are useful in exploring the type (C–H... π , O–H...O, H...H etc.) as well as the proximity of intermolecular contacts in a molecular crystal. The d_{norm} surface ($d_e + d_i$) shows intermolecular contacts relative to the van der Waals radii by way of a simple red, white and blue color scheme: red indicating higher electron density and hydrogen bonding capability and blue representing lower electron density site [23].

Curvedness is a measure of curvature in Hirshfeld surface. Low values of curvedness are associated with essentially flat areas of the surface, while areas of sharp curvature possess a high curvedness and tend to divide the surface into patches associated with contacts between neighboring molecules. The low curvedness suggests close contacts and this is possibly indicative of covalent bonding interactions [24]. The large flat region indicated by a blue outline on the curvedness surfaces indicates π ... π stacking of the molecules. The shape index is the

measurement of shape of Hirshfeld surface. The red triangles on shape index represent concave regions indicating atoms of the $\pi\cdots\pi$ stacked molecule above them and the blue triangles represent convex regions indicating the ring atoms of the molecule inside these surfaces. Figure 9 represents Hirshfeld parameters, curvedness, shape index and d_{norm} and 2D fingerprint plot of ATHTP crystal. Hirshfeld two-dimensional (2D) fingerprint plots offer considerable promise for exploring packing modes and intermolecular interactions in molecular crystals. This analysis allows a quick and easy identification of the significant intermolecular interactions map on the molecular surface. CrystalExplorer, a computer program was used for calculation of Hirshfeld surfaces and 2D fingerprint plots [25].

The larger circular depressions (deep red) visible on the side of the 3D Hirshfeld surfaces correspond to the significant hydrogen bonding contacts. While the red color points indicate the short contacts of H...H, N...H and H...O interactions. The proportion of O...H/H...O interactions covers 37.4% of the total Hirshfeld surfaces with two distinct spikes in the 2D fingerprint plots indicating hydrogen bonding interactions are the most significant interactions in the crystal. The H...H interactions, which are reflected in the middle of scattered points in the 2D fingerprint plot comprise 12.2% of the total Hirshfeld surfaces. Apart from the above interactions, the presence of $\pi\cdots\pi$ (C...C), lone pair... π (N...C, O...C) and lone pair...lone pair (O...O, N...N and O...N) interactions are also observed. The C-H... π interactions also have a small contribution to the total Hirshfeld surfaces of ATHTP.

4.9. z-scan analysis

Z-scan technique is a standard technique for determining the nonlinear index of refraction (n_2) and nonlinear absorption coefficient (β) in solids, liquids. The Z-scan technique is a straight forward method using which the nonlinear optical coefficient can be measured with a high

degree of accuracy. The study of nonlinear refraction by the Z-scan method depends on the position (Z) of the thin sample under investigation along a focused Gaussian laser beam. The sample causes an additional focusing and defocusing depending on whether nonlinear refraction is positive or negative. Measurements of open and closed apertures are shown in Figure 10. The third-order nonlinear optical parameters can be calculated using standard equations [26]. The estimated nonlinear refractive index (n_2) and absorption coefficient (β) and third-order susceptibility (χ^3) of ATHTP crystal are $1.06 \times 10^{-7} \text{ cm}^2/\text{W}$ and $4.05 \times 10^{-4} \text{ cm/W}$ and $2.1 \times 10^{-7} \text{ esu}$ respectively. The positive value of refractive index reveals the self-focusing nature and the β value exhibits the two-photon absorption process and the absolute susceptibility value is due to the π -electron cloud movement from the donor to acceptor which makes the molecule highly polarized [27, 28].

5. Conclusion

Single crystals of 4-amino-4*H*-1,2,4-triazolium styphnate were grown from saturated solution by slow evaporation method at room temperature. Various spectral techniques such as FTIR, ^1H , ^{13}C and DEPT-135 NMR confirmed the molecular structure of ATHTP. The structure of ATHTP was confirmed using single crystal X-ray diffraction studies and ATHTP belong to triclinic system. The crystal structure is stabilized by the presence of various covalent bonds and hydrogen bonds C-H...O, N-H...O and also bifurcated hydrogen bonds. The cut off wavelength of ATHTP from the transmittance spectrum is 290 nm and excitation of luminescence spectrum suggests the suitability of ATHTP crystal for various opto electronic applications and it can be used as a new green-light emitting material. The thermal stability of the title crystal was determined by TG-DTA studies and it can be exploited for any application up to 178°C. The third-order nonlinear optical susceptibility is found to be $2.1 \times 10^{-7} \text{ esu}$. The nonlinear refractive

index indicates that ATHTP exhibits self-focusing optical nonlinearity. Quantum chemical calculations show that the first-order polarizability (β) of synthesized crystal is 3.89×10^{-30} esu. First-order hyperpolarizability (β) of ATHTP is 30 times greater than that of urea. Thus ATHTP can act as a promising material for nonlinear optical applications and it can also possibly be used for the fabrication of electro optic devices. Hirshfeld surface analysis of ATHTP crystal demonstrated that among the different kinds of interactions, O...H is more prominent.

Acknowledgements

One of the authors, Dr. M. Dhandapani, would like to thank the University Grants Commission (UGC), New Delhi, India for the financial support (Major Research Project Grant No. 43-200/2014(SR)) to carry out the research work. P. Dhamodharan, thanks the Dr. R. Nagarajan, School of Chemistry and UGC Networking Centre, Hyderabad, for awarding visiting research fellowship.

References

- [1] (a) A. D. Bond, Chem. Commun. (2002) 1665. (b) M. Kidowaki, N. Tamaoki, Chem. Commun. (2003) 291.
- [2] C. Bouzidi, K. H. Naifer, Z. Khadraoui, H. Elhouichet, M. Ferid, Physica b 497 (2016) 34.
- [3] J. A. Kitchen, A. Noble, C. D. Brandt, B. Moubaraki, K. S. Murray, S. Brooker, Inorg. Chem. 47 (2008) 9450.
- [4] U. Beckmann, S. Brooker, Coord. Chem. Rev. 245 (2003) 17.
- [5] V. Chithambaram, S. Jerome Das, R. Arivudai Nambi, S. Krishnan, Optics & Laser Technology 43 (2011) 1229.
- [6] P. Tanusri, K. Tanusree, B. Gabriele, R. Lara, Cryst. Growth Des. 3 (2003) 13.
- [7] Urbanski, Chemistry and Technology of Explosives, Pergamon press, Oxford-London, Vol. I, 1964.
- [8] G.M. Sheldrick, SHELXS-97, A Program for Solution of Crystal Structures, University of Göttingen, Germany, 1997.
- [9] G.M. Sheldrick, SHELXL-97, A Program for Solution of Crystal Structures, University of Göttingen, Germany, 1997.
- [10] M.J. Frisch *et al.*, Gaussian-09, Revision E. 01, Gaussian, Inc., Wallingford (CT), 2009.
- [11] A. D. Becke, J. Chem. Phys. 98 (1993) 5648.
- [12] A. D. Becke, Phys. Rev. A 38 (1988) 3098.

- [13] C. Lee, W. Yang, R.G. Parr, *Phys. Rev.* 378 (1988) 785.
- [14] *Molecular structures and dimensions* (1972) Vol. A1. Inter atomic distances, 1960-65. Organic and Organometallic Crystal structures.
- [15] H. A. Bent, *J.Inorg. Nucl. Chem.* 19 (1961) 43.
- [16] H.O. Kalinowski, S. Berger, S. Braun, *Carbon-13 NMR Spectroscopy*, John Wiley & Sons, Chichester, 1988.
- [17] N. Mansour, A. Momeni, R. Karimzadeh, M. Amini, *Opt. Mater. Exp.*, 2 (2012) 740.
- [18] E. Selvakumar, G. Anandha babu, P. Ramasamy, Rajnikant, V. Murugesan, A. Chandramohan, *Spectrochim. Acta Part A.* 117 (2014) 259.
- [19] H. O. Kalinowski, S. Berger, S. Braun, *Carbon-13 NMR Spectroscopy*, John Wiley & Sons, Chichester, 1988.
- [20] Robert M. Silverstein, Francis X. Webster, *Spectrometric Identification of Organic Compounds*, sixth ed., J. Wiley & Sons, Chichester, 2004.
- [21] H. K. Fun, M. Hemamalini, B. P. Siddaraju, H. S. Yathirajan, B. Narayana, *Acta Crystallogr. E* 66 (2010) 682.
- [22] Yan-jun Li, *Acta Crystallogr. E* 65 (2009) 2566.
- [23] I. Skovsen, M. Christensen, H. F. Clausen, J. Overgaard, C. Stiewe, T. De gupta, E. Mueller, Spackman, M. A. Iversen, *Inorg. Chem.* 49 (2010) 9343.
- [24] D. Jayatilaka, J. J. McKinnon, M. A. Spackman, *Chem. Commun.* (2007) 3814.
- [25] S. K. Wolff, D. J. Grimwood, J. J. McKinnon, D. Jayatilaka, M. A. Spackman, *Crystal Explorer 2.0*, University of Western Australia, Perth, Australia, 2007.
- [26] K. Naseema, M. Shyma, K.B. Manjunatha, A. Muralidharan, G. Umesh, *Vijayalakshmi Rao, Optics & Laser Technology* 43 (2011) 1286.
- [27] J. J. Rodrigues, J. L. Misogati, F. D. Nunes, R. Mendonca, S. C. Zilioc, *Opt. Mater.* 22 (2003) 23.
- [28] Y. S. Zhou, E. B. Wang, J. Peng, *Polyhedron* 18 (1999) 1419.

Figure 1 Synthesis of styphnic acid and 4-amino-4H-1,2,4-triazol-1-ium-3-hydroxy-2,4,6-trinitrophenolate

Figure 2 Asymmetric unit of the compound with atomic labeling scheme at 50% probability level

Figure 3 Packing diagram of ATHTP along a, b and c axis

Figure 4 UV-Vis-NIR spectrum of ATHTP

Figure 5 Phosphorescence emission spectrum of ATHTP

Figure 6 TG/DTA curves of ATHTP

Figure 7 ^1H and ^{13}C NMR spectra of ATHTP

Figure 8 Optimized molecular structure of ATHTP

Figure 9 Hirshfeld d_{norm} , Shape index, Curvedness and fingerprint plots of ATHTP

Figure 10 Z-scan patterns in open and closed aperture.

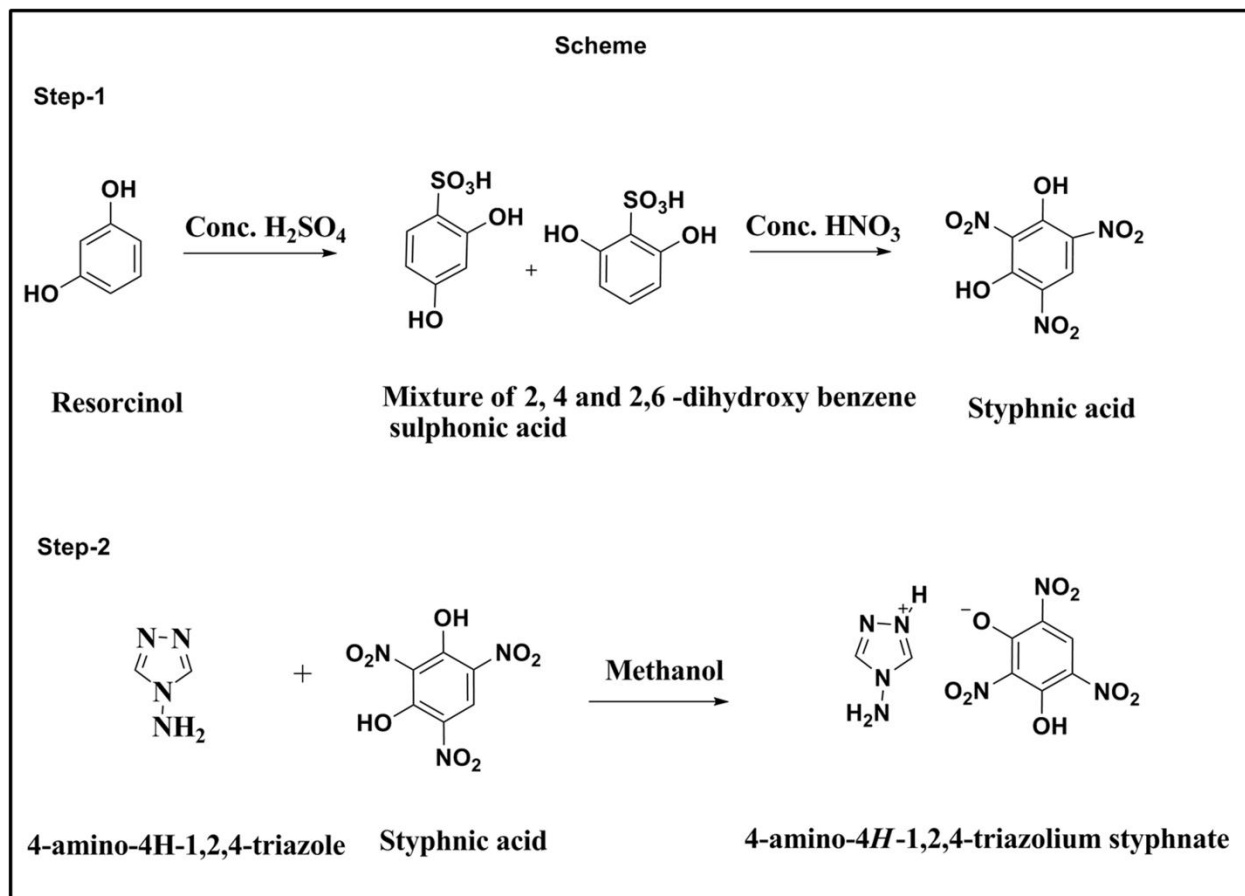


Figure 1

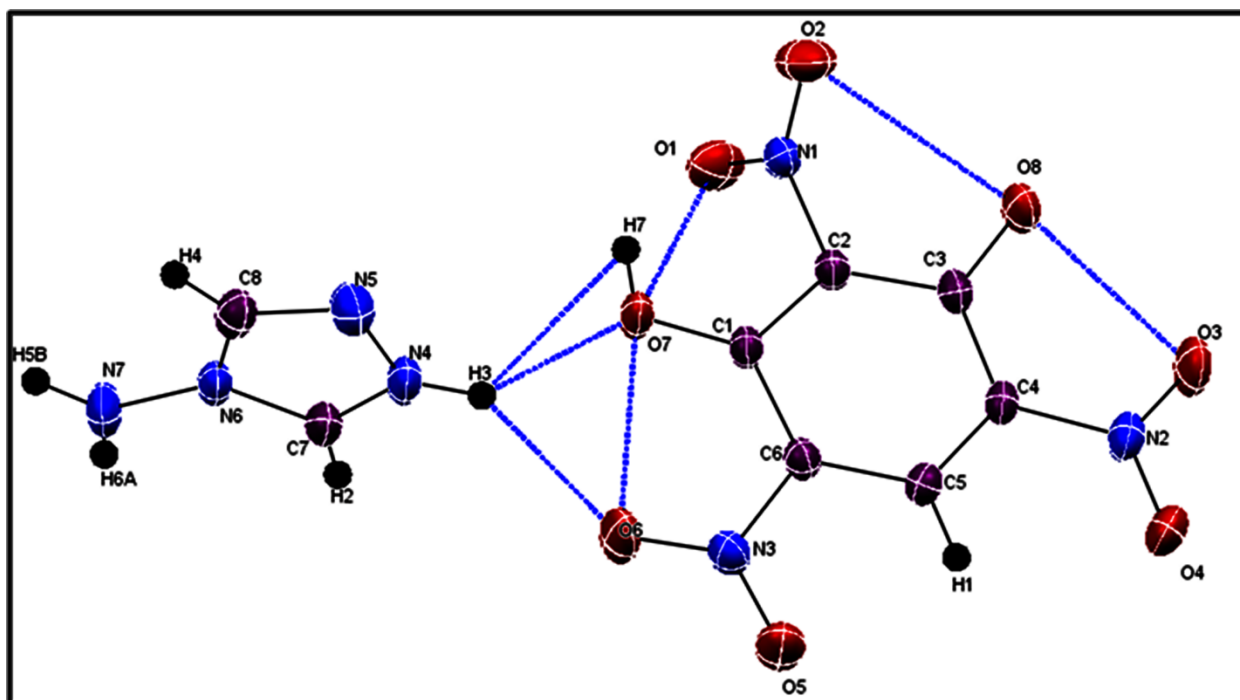


Figure 2

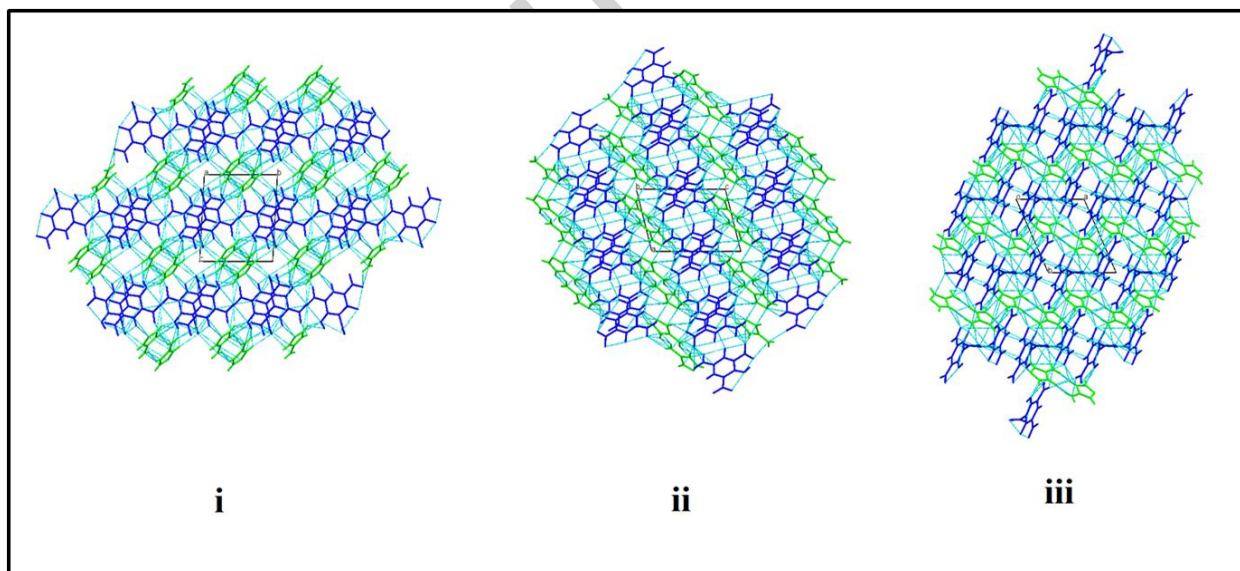


Figure 3

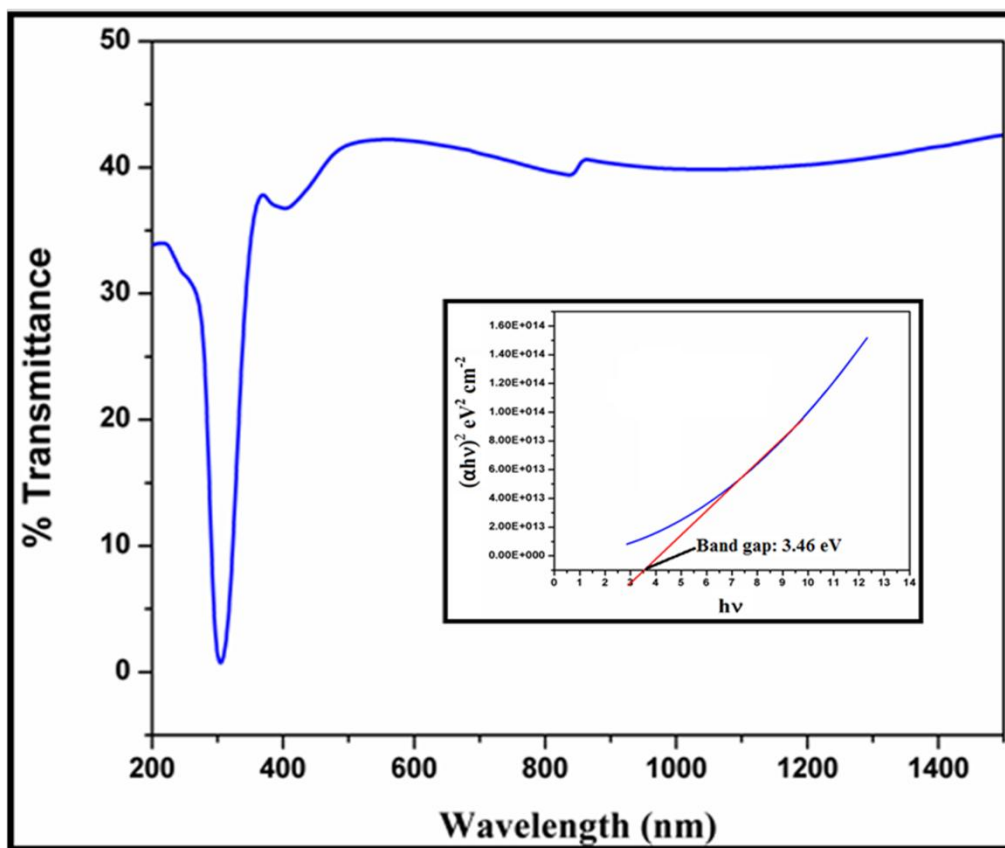


Figure 4

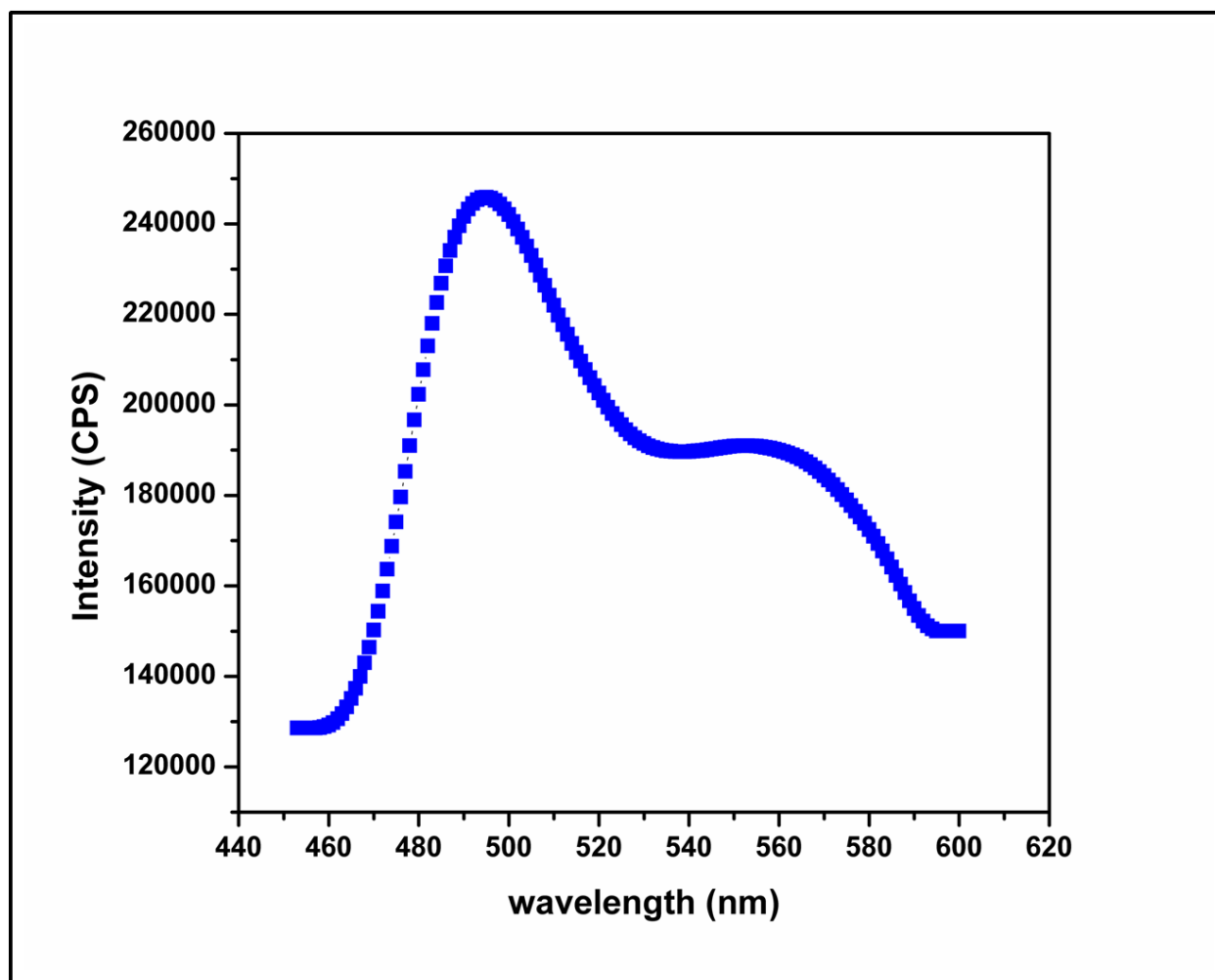


Figure 5

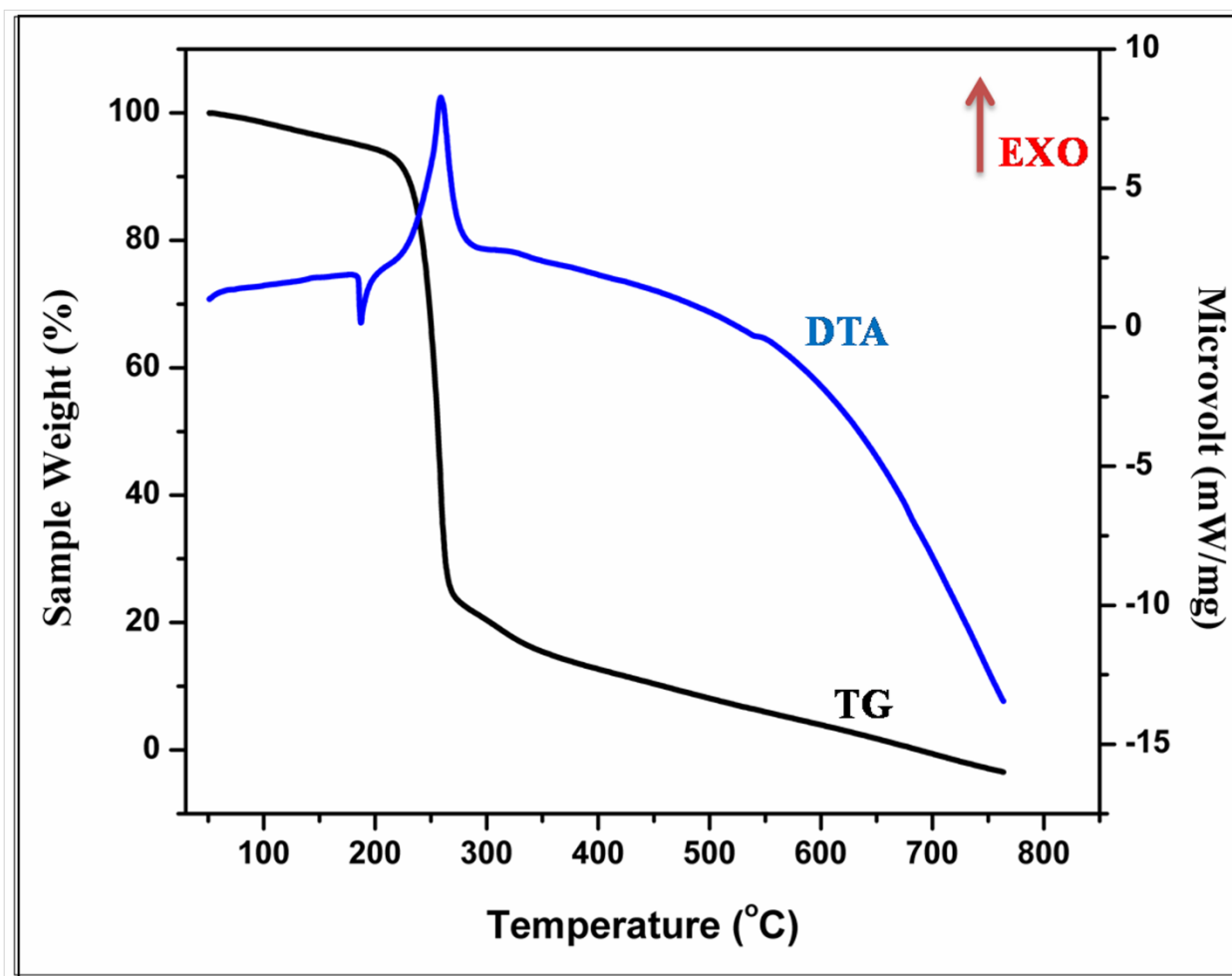


Figure 6

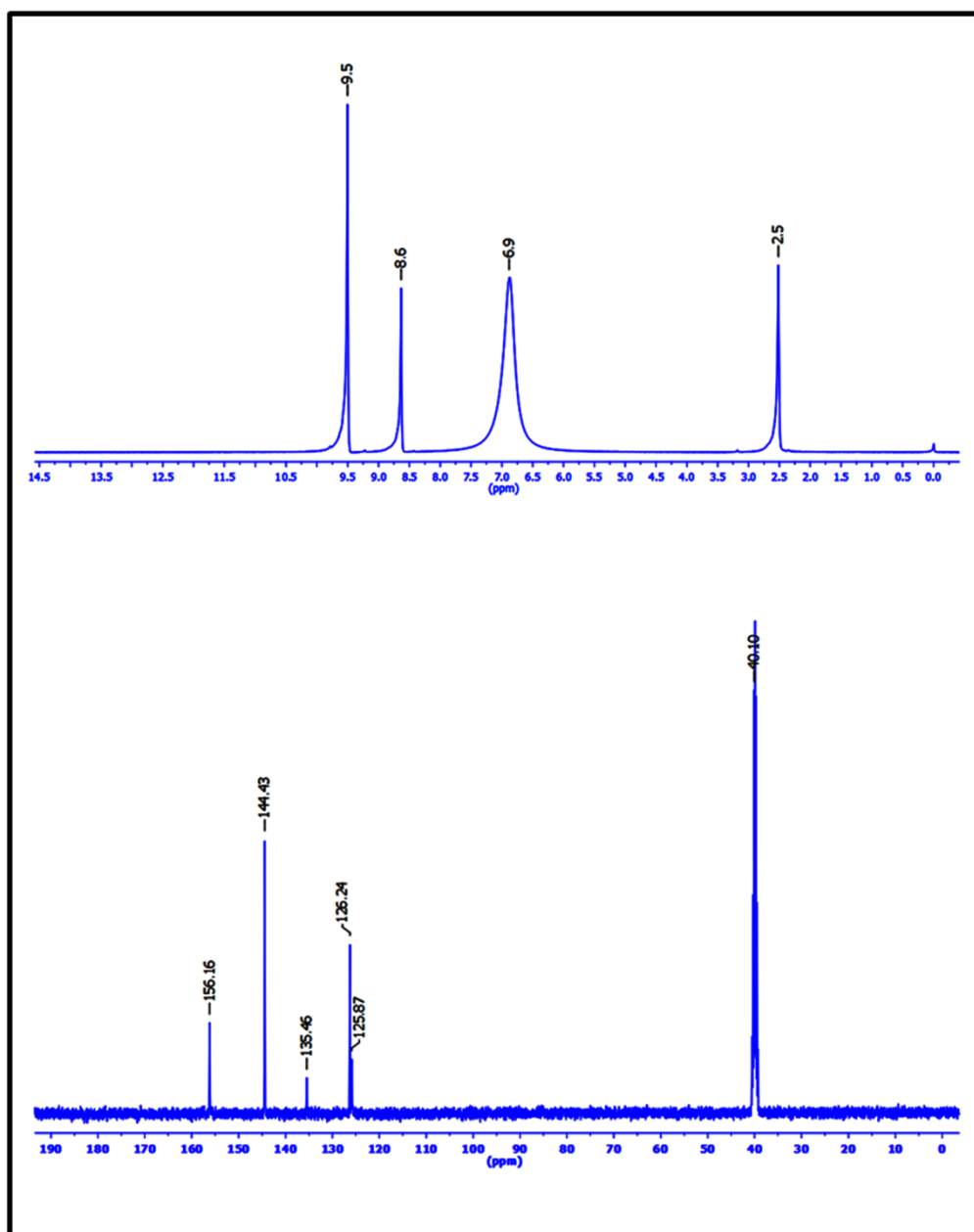


Figure 7

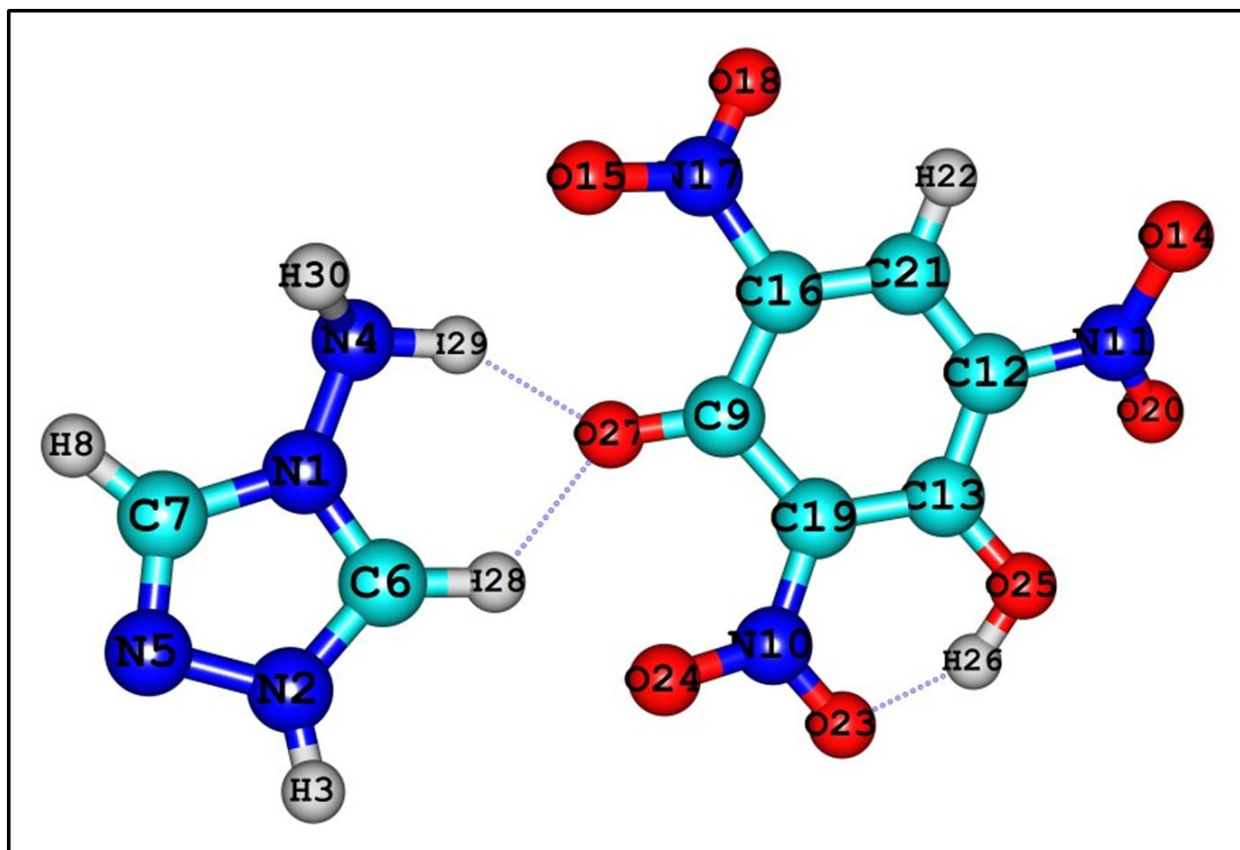


Figure 8

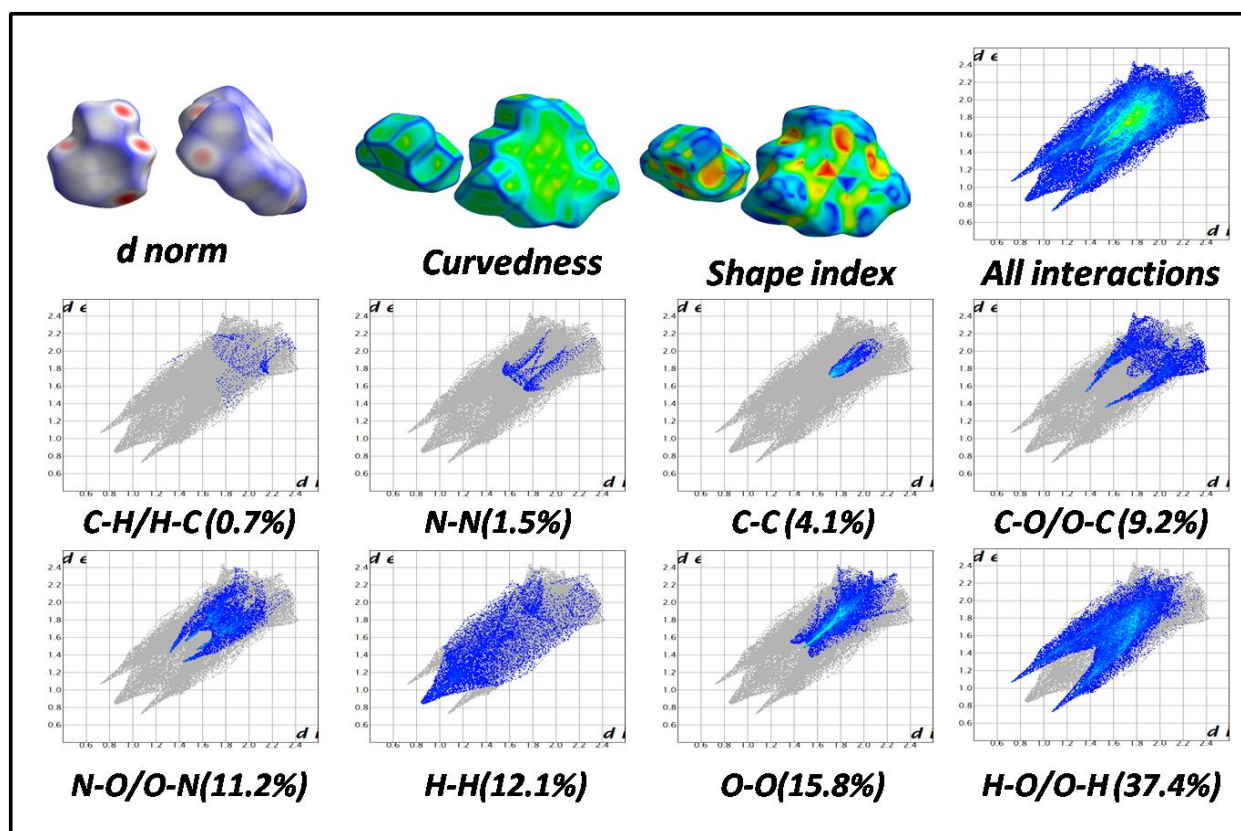


Figure 9

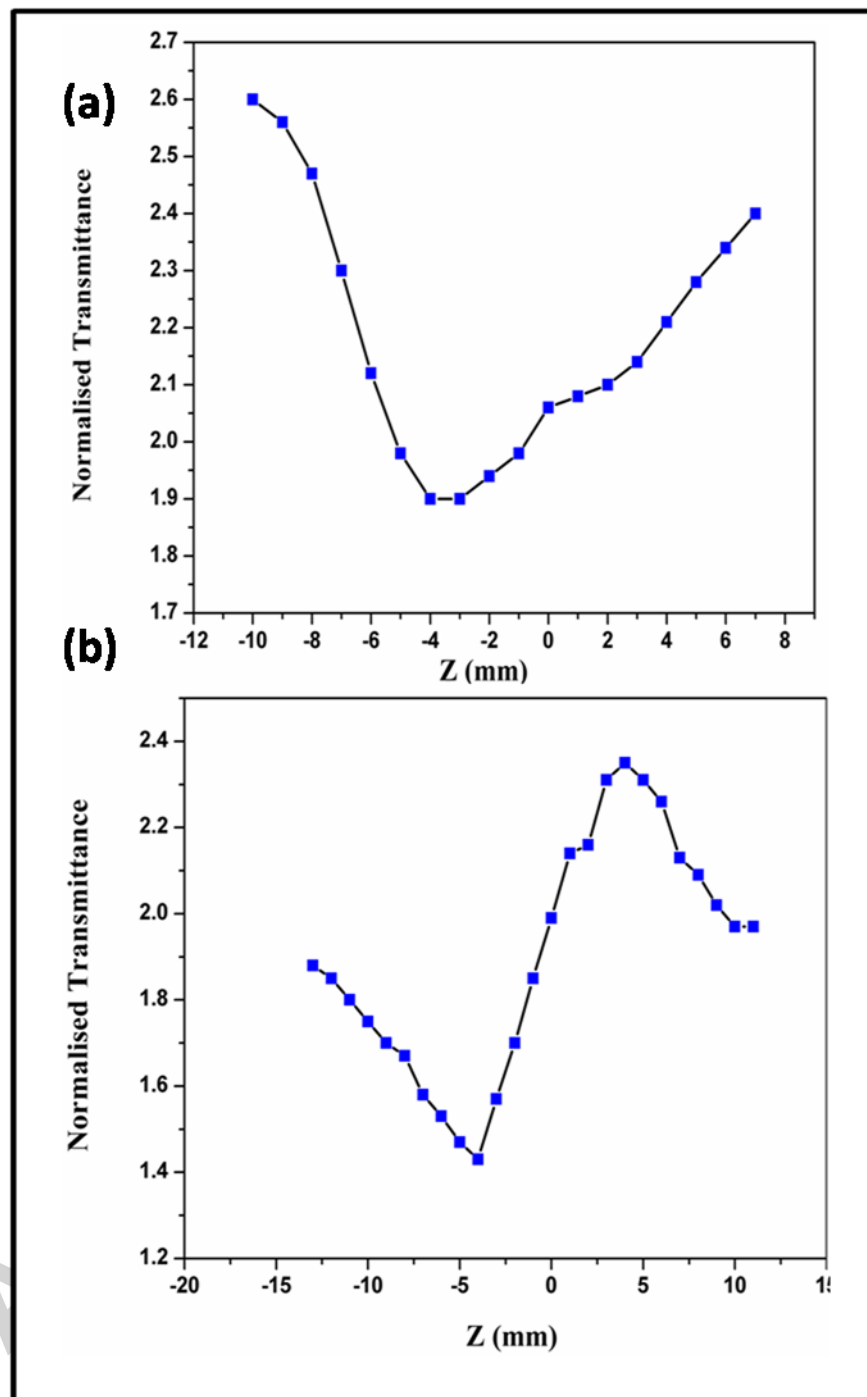


Figure 10

Table 1: Crystal data and structure refinement for ATHTP Crystal

Empirical formula	$C_8 H_7 N_7 O_8$	
Formula weight	329.21	
Temperature	298(2) K	
Wavelength	0.71073 Å	
Crystal system	Triclinic	
Space group	<i>P</i> -1	
Unit cell dimensions	$a = 7.8000(16)$ Å	$\alpha = 87.22(3)^\circ$.
	$b = 8.9000(18)$ Å	$\beta = 75.97(3)^\circ$.
	$c = 9.932(2)$ Å	$\gamma = 66.30(3)^\circ$.
Volume	$611.5(2)$ Å ³	
Z	2	
Density (calculated)	1.788 Mg/m ³	
Absorption coefficient	0.161 mm ⁻¹	
F(000)	336	
Crystal size	0.18 x 0.15 x 0.12 mm	
Theta range for data collection	2.12 to 26.24°.	
Index ranges	-9<=h<=9, -11<=k<=11, -12<=l<=12	
Reflections collected	6459	
Independent reflections	2437 [R(int) = 0.0198]	
Completeness to theta = 26.24°	98.6 %	
Refinement method	Full-matrix least-squares on F^2	
Data / restraints / parameters	2437 / 0 / 210	
Goodness-of-fit on F^2	1.053	
Final R indices [I>2sigma(I)]	R1 = 0.0525, wR ² = 0.1574	
R indices (all data)	R1 = 0.0554, wR ² = 0.1611	
Extinction coefficient	0.097(13)	
Largest diff. peak and hole	0.530 and -0.526 e Å ⁻³	
CCDC:	1034328	

Table 2: Comparison Bond lengths [\AA] and Bond angles [$^\circ$] of ATHTP molecule

Atoms	Observed	Calculated	Atoms	Observed	Calculated
N(6)-C(7)	1.323	1.341	C(7)-N(6)-C(8)	107.07	107
N(6)-C(8)	1.347	1.375	C(7)-N(6)-N(7)	123.14	127.9
N(6)-N(7)	1.399	1.402	C(8)-N(6)-N(7)	129.77	124.7
C(3)-O(8)	1.328	1.246	O(8)-C(3)-C(2)	118.55	122.4
C(3)-C(2)	1.367	1.469	O(8)-C(3)-C(4)	124.92	123.5
C(3)-C(4)	1.407	1.449	C(2)-C(3)-C(4)	116.52	113.9
N(1)-O(1)	1.205	1.257	O(1)-N(1)-O(2)	122.8	119.7
N(1)-O(2)	1.206	1.232	O(1)-N(1)-C(2)	118.57	119
N(1)-C(2)	1.449	1.424	O(2)-N(1)-C(2)	118.59	121.2
N(3)-O(5)	1.212	1.222	O(5)-N(3)-O(6)	122.31	124.6
N(3)-O(6)	1.213	1.230	O(5)-N(3)-C(6)	118.09	116.7
N(3)-C(6)	1.443	1.464	O(6)-N(3)-C(6)	119.6	118.6
O(4)-N(2)	1.208	1.227	C(5)-C(6)-C(1)	122.47	120.9
C(4)-C(5)	1.377	1.377	C(5)-C(6)-N(3)	116.73	117
C(4)-N(2)	1.417	1.454	C(1)-C(6)-N(3)	120.78	121.9
N(2)-O(3)	1.241	1.234	O(7)-C(1)-C(2)	120.49	122.8
N(4)-C(7)	1.296	1.329	O(7)-C(1)-C(6)	127.32	119.5
N(4)-N(5)	1.357	1.357	C(2)-C(1)-C(6)	112.19	117.5
N(5)-C(8)	1.293	1.304	C(5)-C(4)-C(3)	120.05	122.1
C(6)-C(5)	1.365	1.387	C(5)-C(4)-N(2)	119.09	116.9
C(6)-C(1)	1.434	1.412	C(3)-C(4)-N(2)	120.84	120.8
C(1)-O(7)	1.246	1.316	O(4)-N(2)-O(3)	121.59	118
C(1)-C(2)	1.418	1.431	O(4)-N(2)-C(4)	120.33	118.6
C(1)-C(2)-N(1)	115.75	112.9	N(5)-C(8)-N(6)	111.1	111.1
C(8)-N(5)-N(4)	103.51	103.6	O(3)-N(2)-C(4)	118.08	122.7
N(4)-C(7)-N(6)	106.3	105.2	C(3)-C(2)-C(1)	127.21	118.8
C(6)-C(5)-C(4)	121.55	121.9	C(3)-C(2)-N(1)	117	118.4
C(7)-N(4)-N(5)	112.09	121.9			

RMSD values for Bond lengths and Bond angles are 0.03821 \AA and 3.413 $^\circ$, respectively.

*Calculated from optimized structure from DFT.

Table 3: Comparison of static first hyperpolarizability for the constituents of ATHTP

Hyperpolarizability tensor	Styphnic acid	4-amino-4H-1,2,4-triazole	ATHTP
xxx	0.0047	-46.595	-381.98
yyy	-21.5119	0.0017	-58.17
zzz	-0.0001	0.0001	1.299
xyy	-0.004	-15.3840	-50.47
xyx	47.9402	0.000	16.379
xxz	0.0032	-0.0001	8.116
xzz	-0.0003	0.3413	3.047
yyz	-11.4252	0.0001	-2.398
yyx	-0.0010	0.0007	11.283
xyz	3.6845	-0.0001	-15.190
β_{total}	0.1295×10^{-30} esu	0.535×10^{-30} esu	3.89×10^{-30} esu

Highlights

- Single crystals were grown by slow evaporation solution growth technique.
- N-H...O, O-H...O and C-H...O type of interactions lead to stable network.
- The thermal stability of the compound was investigated by TG/DTA analyses.
- The third-order nonlinear optical susceptibility is found to be 2.1×10^{-7} esu.
- Hirshfeld analyses explore covalent and non covalent interactions.